HHS Public Access

Author manuscript

J Mol Cell Cardiol. Author manuscript; available in PMC 2019 January 01.

Published in final edited form as:

J Mol Cell Cardiol. 2018 January ; 114: 288–299. doi:10.1016/j.yjmcc.2017.12.003.

Transverse tubular network structures in the genesis of intracellular calcium alternans and triggered activity in cardiac cells

Zhen Song[1,*], **Michael B. Liu**[1], and **Zhilin Qu**[1,2,*]

[1]Department of Medicine, David Geffen School of Medicine, University of California, Los Angeles, California 90095, USA

[2]Department of Biomathematics, David Geffen School of Medicine, University of California, Los Angeles, California 90095, USA

Abstract

Rationale—The major role of a transverse-tubular (TT) network in a cardiac cell is to facilitate effective excitation-contraction coupling and signaling. The TT network structures are heterogeneous within a single cell, and vary between different types of cells and species. They are also remodeled in cardiac diseases. However, how different TT network structures predispose cardiac cells to arrhythmogenesis remains to be revealed.

Objective—To systematically investigate the roles of TT network structure and the underlying mechanisms in the genesis of intracellular calcium (Ca^{2+}) alternans and triggered activity (TA).

Methods and Results—Based on recent experimental observations, different TT network structures, including uniformly and non- uniformly random TT distributions, were modeled in a cardiac cell model consisting of a three-dimensional network of Ca^{2+} release units (CRUs). Our simulations showed that both Ca^{2+} alternans and Ca^{2+} wave-mediated TA were promoted when the fraction of orphaned CRUs was in an intermediate range, but suppressed in cells exhibiting either well-organized TT networks or low TT densities. Ca^{2+} alternans and TA could be promoted by low TT densities when the cells were small or the CRU coupling was strong. Both alternans and TA occurred more easily in uniformly random TT networks than in non-uniformly random TT networks. Subcellular spatially discordant Ca^{2+} alternans was promoted by nonuniformly random TT networks but suppressed by increasing CRU coupling strength. These mechanistic insights provide a holistic understanding of the effects of TT network structure on the susceptibility to arrhythmogenesis.

[*]Correspondence to: Zhilin Qu, PhD, Department of Medicine, Division of Cardiology, David Geffen School of Medicine at UCLA, A2-237 CHS, 650 Charles E. Young Drive South, Los Angeles, CA 90095, Tel: 310-794-6050, Fax: 310-206-9133, zqu@mednet.ucla.edu. Zhen Song, PhD, Department of Medicine, Division of Cardiology, David Geffen School of Medicine at UCLA, A2-237 CHS, 650 Charles E. Young Drive South, Los Angeles, CA 90095, zsong@mednet.ucla.edu.

Conclusions—The TT network plays important roles in promoting Ca^{2+} alternans and TA, and different TT network structures may predispose cardiac cells differently to arrhythmogenesis.

Keywords

T-tubules; cell size; calcium cycling; alternans; triggered activity

Introduction

Transverse tubules (TTs) are sarcolemma membrane invaginations of skeletal and cardiac muscle cells. The TTs also branch into axial tubules (ATs), forming a TT network inside the cell [1–3]. The major role of a TT network in a cardiac myocyte is to facilitate effective excitation-contraction (E-C) coupling and signal transduction [4–6]. The TT network structure is very heterogeneous within a cardiac cell and also varies across different types of the heart cells [4, 7, 8], which may undergo remodeling in diseases, such as ischemia and heart failure [2, 9–16]. For example, a normal ventricular myocyte (VM) consists of a well-structured high-density TT network (Fig. 1A) [1, 2], which are remodeled in hypertension and heart failure to have a reduced TT density due to TT disruption [2, 10–15]. The remodeled TT networks become more heterogeneous, which include patchy (Fig. 1B) [2, 11] and sheet-like (Fig. 1C) [15] structures. Unlike those in VMs, the TT networks in atrial myocytes (AMs) are usually much less dense than those in VMs (Fig. 1D) [3]. Studies also have shown that the TT networks in AMs are very heterogeneous between regions in the same heart [17–20] and between species [21]. Some AMs exhibit well-organized TT structures, similar to those in VMs, while other AMs exhibit sparse TT networks such as the one shown in Fig. 1D, and some AMs even completely lack TTs. Purkinje cells (P-cells) are largely free of TTs [7, 22, 23]. TTs are also largely absent in myocytes in early development, in cultured myocytes, and in stem-cell derived cardiac myocytes [4, 24–27].

Under normal conditions, different types of cardiac cells exhibit different types of TT network structures, which may reflect their fitness for E-C coupling and signaling in the heart. For example, the main role of a P-cell is to facilitate fast conduction, and thus lacking a TT network is an advantage since a smaller membrane capacitance or surface-to-volume ratio results in a faster conduction. On the other hand, the main role of a VM is to facilitate robust contraction, and a dense TT network is needed for synchronous calcium (Ca^{2+}) release. If the TT network is uniformly dense, the efficacy of E-C coupling and signaling does not depend on cell size since the Ca^{2+}-dependent ion channels, such as L-type Ca^{2+} channels (LCCs) and Na^{+}-Ca^{2+} exchange (NCX), are distributed everywhere inside cells. However, when the TT network becomes sparse and heterogeneous, the efficacy will depend on cell size. For example, in the absence of a TT network, a smaller cell can have a better E-C coupling efficacy since it is easier for the LCCs on the sarcolemmal membrane to trigger a more synchronous whole-cell Ca^{2+} release. The TT network structure may also correlate with RyR cluster density (or spacing) in a cell since ryanodine receptor (RyR) clusters tend to colocalize with LCC clusters. For example, the average RyR cluster distance in normal VMs is larger than in AMs [28], and much larger than in sino-atrial nodal (SAN) cells [29]. A closer RyR cluster spacing promotes Ca^{2+} waves and Ca^{2+} oscillations [29–32], which facilitates Ca^{2+} clocks for normal SAN function but is arrhythmogenic in VMs. While

different TT network structures may be optimized for their needs in normal cardiac functions, these differences may also predispose the cardiac cells differently to arrhythmogenesis under cardiac diseases. Moreover, remodeling of the TT network in cardiac diseases may further potentiate arrhythmogenesis, such as TT disruption in heart failure promoting intracellular Ca^{2+} alternans [33]. However, the roles of TT network structures and the underlying arrhythmogenic mechanisms remain to be elucidated [34].

In this study, we investigate the roles of TT network structures in the genesis of intracellular Ca^{2+} alternans and Ca^{2+}-wave mediated triggered activity (TA) using computational modeling. A three-dimensional (3D) cell model consisting of a network of Ca^{2+} release units (CRUs) was used [35–37]. Different TT network structures were simulated, including uniformly random structures (Fig. 1E), patchy structures (Fig. 1F), hollow structures (Fig. 4B and Fig. S3), and sheet- like structures (Fig. 1G). We showed that both Ca^{2+} alternans and Ca^{2+} wave- mediated TA were promoted when the fraction of orphaned CRUs (OCRUs) was in an intermediate range, but suppressed in cells with well-organized TT networks (low OCRU ratios) or low TT densities (high OCRU ratios). Ca^{2+} alternans and TA could be promoted by low TT densities when the cells are small or the CRU coupling is strong. Both alternans and TA occurred more easily in uniformly random than in non-uniformly random TT networks under the same OCRU ratio. Subcellular spatially discordant Ca^{2+} alternans was promoted by non-uniform TT networks but suppressed by increasing CRU coupling strength. These mechanistic insights provide a holistic understanding of how TT networks affect the susceptibility to arrhythmogenesis.

Methods

Cell model

The cell model consisted of an action potential (AP) model with detailed spatiotemporal Ca^{2+} cycling described by a 3D network of CRUs, which was detailed in our previous studies [35–37] and briefly described in Supplemental Information. The parameter changes used to induce Ca^{2+} alternans and TA were shown in Tables S1 and S2, respectively. The control size of the cell was $L_x \times L_y \times L_z = 64 \times 32 \times 16$ CRUs. We used $L_x = 64$ CRUs and $L_y = 32$ CRUs but varied L_z to study the effects of cell size. The LCC cluster size, i.e., the number of LCCs (n_{LCC}) in each CRU, was 6, but was varied to investigate the effects of LCC cluster size on alternans and TA.

TT network model

The main role of the TT network in a cardiac cell is to allow ion channels to distribute spatially inside the cell volume. Since our focus in this study was Ca^{2+} cycling dynamics, we distributed the LCC clusters and NCX (or LCC-NCX clusters) spatially according to the TT network structure. That is, whenever a CRU is associated with a sarcolemmal or tubular membrane, it has a LCC-NCX cluster. A CRU without a LCC-NCX cluster is called an OCRU [2]. The CRUs in the outermost layer which are proximal to the sarcolemmal membrane were always coupled to LCC-NCX clusters (see Fig. S1). We assumed that the Ca^{2+}-independent ion currents were uniformly distributed in the CRUs and thus the corresponding current densities were independent of TT network structures.

We simulated different characteristic TT network structures, and the algorithms generating these structures are described in detail in online Supplemental Information. Here we describe them briefly. *Random TT networks* (e.g., Fig. 1E): This type of TT network structures was generated by a uniformly random spatial distribution of the LCC-NCX clusters on the CRUs inside the cell. *Patchy and hollow TT networks*: These TT network structures were generated using random walks starting from random locations on cell membrane. We can generate various non-uniformly random TT structures with different AT-to-TT ratios and densities by varying the probabilities for the six walking directions, the total number of random walks, and the length of each walk. When the walk length is long, the random walks can cover the whole cell volume, resulting in patchy TT networks (e.g., Fig. 1F). When the walk length is short, the random walks only cover the space proximal to the cell membrane with the majority of CRUs in the center region being OCRUs, which results in hollow TT networks (see Fig. 4B and Fig. S3). *Random T-sheet structures* (e.g., Fig. 1G): T-sheets were generated by randomly growing from the two sides (y-direction) of the outermost layer to form sheet- like TT structures, which exhibit irregular lengths and shapes.

In a higher TT density network, the percentage of OCRUs is lower, and vice versa. One can define an OCRU ratio in a cell as the number of OCRUs against the total CRUs, i.e.,

$$\phi_{total}=\frac{Number\ of\ OCRUs}{L_x L_y L_z} \quad (1)$$

However, this ratio depends on cell size since none of the CRUs in outermost layer are OCRUs. To define a size-independent OCRU ratio ϕ, we exclude the CRUs in the outermost layer, i.e.,

$$\phi=\frac{Number\ of\ OCRUs}{(L_x-2)\times(L_y-2)\times(L_z-2)} \quad (2)$$

Therefore, ϕ ranges between 0 and 1 (or 0 and 100%), independent of cell size. ϕ=1 indicates that all CRUs inside the cell except those in the outermost layer are OCRUs, i.e., TTs are absent in the cell. We used $\eta \propto \frac{D}{d^2}$ as a parameter describing CRU coupling strength determined by CRU spacing (d) and Ca^{2+} diffusion constant (D). A smaller η corresponds to a weaker CRU coupling.

Pacing protocol

For the simulations of Ca^{2+} alternans, the cell was paced by a clamped AP (see Fig. S5) to avoid the effects of Ca^{2+} and voltage coupling on Ca^{2+} alternans. For the simulations of TA, the cell was paced by a current pulse of 2 ms with an amplitude of −50 pA/pF (current-clamp mode). We paced 40 beats at a pacing cycle length (PCL) of 300 ms for the cell to

reach steady state, and then stopped pacing to allow delayed afterdepolarizations (DADs) and TA to occur.

Results

We carried out simulations with uniformly and non-uniformly random TT networks to investigate their effects on the genesis of Ca^{2+} alternans and TA. We first used the uniformly random TT network to investigate the effects of TT density, cell thickness, and CRU coupling on the genesis of whole-cell Ca^{2+} alternans as well as subcellular spatially discordant Ca^{2+} alternans. We then explored how different non- uniformly random TT network structures, including patchy, hollow and T-sheet structures, affect the alternans dynamics. Next, we performed simulations to investigate the genesis of TA with different TT network structures. Finally, since both LCC and NCX strengths play important roles in Ca^{2+} cycling dynamics, we also varied the LCC cluster size and NCX magnitude to investigate the roles of their interactions with the TT network structures in the genesis of Ca^{2+} alternans and TA. The underlying mechanisms linking the subcellular structures to the cellular dynamics are discussed in detail in the Discussion.

Dependence of Ca^{2+} alternans on TT density and cell thickness

Ca^{2+} alternans was induced by fast pacing with control RyR open probability and SERCA activity (Table S1). We first used uniformly random TT network distributions to investigate the effects of TT density by scanning ϕ from 0 to 100% (e.g., from no OCRUs to 100% OCRUs inside the cell). Agreeing with experimental observations, reducing the TT density resulted in a decrease in Ca^{2+} transient but a small or almost no increase in SR Ca^{2+} load depending on the leakiness of RyRs (Fig. S6). Ca^{2+} alternans occurred as PCL became shorter and when ϕ was in an intermediate range, and was suppressed when ϕ was either low or high (Figs. 2A and B). Increasing ϕ also caused alternans to occur at slower pacing rates (Fig. 2C). For example, for the case in Fig. 2C, increasing ϕ from 30% to 50% shifted the onset of alternans from PCL=380 ms to 440 ms. Increasing CRU coupling strength (by increasing η) promoted alternans by increasing both the amplitude of alternans and the range of ϕ values exhibiting alternans (Fig. 2B).

The occurrence of alternans is also cell size dependent. In Fig. 2D, we show the occurrence of Ca^{2+} alternans (gray boxes) versus cell thickness (L_z) and ϕ. When the cell is thick, the alternans regime is insensitive to thickness. However, once the cell is relatively thin, the alternans regime moves toward a higher range of ϕ as the cell becomes thinner.

To avoid the confluent effect of voltage on Ca^{2+} alternans, we used a clamped AP waveform to pace the cell. However, when we used the current clamp mode (i.e., free running AP), the same Ca^{2+} alternans behavior still held (see Fig. S7A). In our simulations, although the Ca^{2+} alternans amplitude can be very large, the AP alternans is small. This is because a larger Ca^{2+} transient causes a larger I_{NCX} but a smaller $I_{Ca,L}$ due to a stronger Ca^{2+}-dependent inactivation (see Fig. S7B), and thus a large change in Ca^{2+} transient only results in a small change in AP. Similar recordings have been shown in experiments [38].

Spatially discordant Ca^{2+} alternans

Both spatially concordant (Fig. 3A) and discordant (Fig. 3B) alternans were observed in our simulations. Since we used the same initial condition for all simulations but a different random TT network for each simulation, the discordant alternans patterns were random (see examples in Fig. 3B). Therefore, the TT network structure plays an important role in the formation of discordant alternans.

The occurrence of discordant alternans depends on TT density, CRU coupling, and cell size. For the control CRU coupling strength (η=1.43) and when ϕ=30% (Fig. 3C), we did not observe discordant alternans but only concordant alternans. When ϕ=50%, about 40% of the simulations gave rise to discordant alternans. When ϕ=70%, the instances of discordant alternans reduced to 20%. Increasing the CRU coupling strength (η=2, Fig. 3D) reduced the likelihood of discordant alternans. This is because a stronger CRU coupling enhances CRU synchronization, which promotes concordant alternans. As cell thickness was reduced, the likelihood of discordant alternans first increased and then decreased (Fig. 3E).

Effects of heterogeneous TT network structures on Ca^{2+} alternans

To investigate the effects of TT network heterogeneities on Ca^{2+} alternans, we used three characteristic non-uniform TT network structures (see Methods): patchy (Fig. 4A), hollow (Fig. 4B), and sheet- like (Fig. 4C) TT network structures. The left panel in Fig. 4A is a patchy TT network pattern, where ϕ=~50%. We also used an AT-to-TT ratio of 3, which is similar to what was observed in atrial myocytes in experiments [3]. When the control CRU coupling strength (η=1.43) was used, no alternans was observed for any ϕ value. This is in contrast to the uniformly random TT networks in which alternans was observed at control CRU coupling strength. When η was increased to enhance CRU coupling, alternans occurred in intermediate ranges of ϕ (middle panel in Fig. 4A). Increasing the AT-to-TT ratio while keeping ϕ constant tended to suppress alternans (right panel in Fig. 4A). This is consistent with the fact that more ATs in the cell results in lower densities of TTs in the center of the cell (see Fig. S3 in Supplemental Information). For the hollow TT networks (Fig. 4B), the occurrence of alternans required an even larger η (alternans occurred in η=3.33 not in η=2, middle panel in Fig. 4B). Similarly, increasing the AT-to-TT ratio also suppressed alternans (right panel in Fig. 4B). For the T-sheet structures (Fig. 4C), alternans also tended to occur in an intermediate range of ϕ but required a larger η (right panel in Fig. 4C) than in the uniformly random TT networks.

We then compared the effects of different TT network structures on the formation of discordant alternans (Fig. 4D). For a fair comparison, we kept the OCRU ratio roughly the same (ϕ=~50%) for each TT network structure. η=2 and 3.33 were used since no alternans occurred for the non-uniform TT networks for the control η (=1.43). When η=2, all alternans observed were concordant for uniformly random TT networks, but both concorant and discordant alternans were observed for patchy and sheet-like TT network structures. No alternans occurred for the hollow structures when η=2. When η=3.33, only concordant alternans was observed for all structures, agreeing with the fact that stronger CRU coupling promotes synchronization of CRU firing. Therefore, discordant alternans tends to be

promoted by non-uniform TT networks. However, the effect is mixed as the requirement of a larger η for alternans to occur in these networks also suppresses discordant alternans.

Effects of TT network structure on Ca^{2+} waves and triggered activity

To induce Ca^{2+} waves and TA in the cell, we increased the RyR leakiness, n_{LCC}, NCX strength, and doubled the SERCA activity (Table S2) from their control values in all simulations. We first simulated uniformly random TT network structures. Fig. 5A shows voltage, line scans of local cytosolic Ca^{2+} concentration, $[Ca^{2+}]_i$, and $[Ca^{2+}]_{SR}$ versus time when ϕ=0 (no OCRUs). After the pacing was stopped, one DAD occurred whose magnitude was too small to elicit an AP. When ϕ=50%, three spontaneous APs occurred followed by one DAD (Fig. 5B). When ϕ=100%, there was only one spontaneous AP (Fig. 5C). However, in this case, Ca^{2+} waves continued to occur after the TA was terminated but became less synchronous, propagating from the cell borders to the center. Due to less synchronous Ca^{2+} releases, the resulting DADs were too small to elicit APs. Note that the SR Ca^{2+} load immediately before a triggered AP was lower for larger ϕ (red dashed line), indicating that the triggered APs did not simply result from SR load elevation in these simulations, but rather was promoted by the structural changes of the TT network itself.

The genesis of TA depends not only on ϕ but also on cell thickness. Fig. 5D shows the average number of triggered APs ($<N_{T\ AP}>$) versus ϕ and cell thickness. In general, there were more triggered APs in thicker cells except for very large ϕ (>80%). The range in which triggered APs occurred shifted toward larger ϕ for thinner cells. For very large ϕ (e.g., 100%), more triggered APs occurred in thinner cells. In addition, increasing CRU coupling strength resulted in an increased $<N_{T\ AP}>$ (Fig. 5E) since a stronger CRU coupling potentiates Ca^{2+} waves [29–32].

We then investigated the effects of non- uniform TT network structures on the genesis of TA. Fig. 5F shows $<N_{T\ AP}>$ for four types of TT network structures. For comparison, we kept the ϕ roughly the same (~50%). The uniformly random TT network gave rise to the largest number of triggered APs (mean 3.8, standard deviation 0.4), while the non-uniform TT structures each only ever exhibited one triggered AP.

Effects of LCC cluster size and NCX strength on alternans and triggered activity

Although we showed in Figs. 2 and 4 that alternans tends to occur at intermediate or low ϕ values, alternans can still occur when ϕ=0 by reducing the LCC cluster size or conductance. For the control LCC conductance used in this study, alternans only occurred in a small range of LCC cluster size n_{LCC} (from 2 to 4 in Fig. 6A). Alternans was suppressed when n_{LCC}>4 (note: our control n_{LCC}=6). When the LCC conductance was reduced by 50% (thus the total Ca^{2+} current density of the cell was reduced by 50%), alternans occurred in a much wider range of n_{LCC} (from 2 to 14), but was still suppressed when n_{LCC}>14. The underlying mechanism has been described in our previous studies [39, 40], and reiterated in Discussion of this study. No discordant alternans were observed for either the control or the reduced LCC conductance (Fig. 6B).

When ϕ=50%, the total Ca^{2+} current was reduced by ~40%. In contrast to the case of ϕ=0 shown in Fig. 6A, increasing n_{LCC} always promoted alternans in this case. As shown in Fig.

6C, as N_{LCC} was increased from 3 to even as high as 35, the magnitude of alternans became continuously larger. In addition, discordant alternans was observed (Fig. 6D). The percentage of discordant alternans first increased and then decreased against N_{LCC}.

We then investigated the effects of LCC cluster size and NCX strength on the genesis of TA. Fig. 7A shows $<N_{T\ AP}>$ versus n_{LCC} for three ϕ values. When ϕ=0 (no OCRUs), no TA was observed in the entire range of n_{LCC} simulated. When ϕ=50%, $<N_{T\ AP}>$ increased with n_{LCC} and the SR load remained roughly unchanged (Fig. 7B). When ϕ=100%, TA was observed between n_{LCC}=6 and 11, and only one triggered AP occurred after the pacing stopped in each case. We also simulated the effects of n_{LCC} for a thin cell (Fig. 7C). In this case, $<N_{T\ AP}>$ for ϕ=100% (green circles) was larger than that for ϕ=50% (red circles), until n_{LCC} became very large (N_{LCC} >14). Note that when ϕ=100%, $<N_{T\ AP}>$ was larger in the thin cell than in the thick cell, but when ϕ=50%, $<N_{T\ AP}>$ was much smaller in the thin cell.

To study the effects of NCX on TA, we scanned the NCX magnitude (v_{NCX}) and n_{LCC} for occurrence of TA and spontaneous Ca^{2+} transients. When ϕ=0 (Fig. 7D), the average number of spontaneous Ca^{2+} transients ($<N_{SCaT}>$) decreased from 7 to 1 as v_{NCX} increased from 0.2 to 1 (upper panel). However, we only observed TA for n_{LCC}>10 and in a narrow range of v_{NCX} (lower panel). No TA occurred for either small or large v_{NCX}. When ϕ=50% (Fig. 7E), $<N_{SCaT}>$ decreased from 13 to 1 as v_{NCX} increased from 0.2 to 1.8 (upper panel), and many more triggered APs occurred in a much wider range of v_{NCX} (lower panel). Therefore, NCX plays a dual competing role in generating TA: increasing NCX potentiates depolarization but suppresses spontaneous Ca^{2+} release, and TA only occurs in an optimal NCX range.

Discussion

In this study, we investigated the effects of TT network structure on the genesis of Ca^{2+} alternans and Ca^{2+} wave-mediated TA. We found that when the cell was thick, both alternans and TA were promoted in an intermediate range of OCRU densities, but were suppressed by either low or high OCRU densities. When the cell was thin, alternans and TA could still occur at high OCRU densities. Both alternans and TA occurred more easily in uniformly random TT networks than in non-uniform TT networks. Spatially discordant alternans was promoted by nonuniform TT networks, but supressed by strong CRU coupling. In the sections below, we discuss the role of TT network structure in the genesis of Ca^{2+} alternans and Ca^{2+}-mediated TA, and their susceptibility to arrhythmogenesis in different types of cardiac cells and remodeling of cardiac diseases.

TT network structures and mechanisms of Ca^{2+} alternans

Basic theory of Ca^{2+} alternans—Theories that mechnistically link individual CRU firings to the whole-cell Ca^{2+} alternans have been developed previously [33, 39, 40] and a more complete theory has also been recently proposed [41]. These theories show that two parameters are key to the genesis of alternans: 1) the probability (α) of a primary spark ratio, which is the portion of CRU firings triggered by LCC openings; and 2) the probability (γ) of a primary spark recruiting a neighboring CRU to fire, which is mainly determined by Ca^{2+} level in the cytosol, Ca^{2+} diffusion rate, and the spacing between CRUs. Alternans occurs

when γ is high and α is in the intermediate range (gray region in Fig. 8A). Here we discuss how TT network structure, CRU coupling, and LCC clustering affect Ca^{2+} alternans based on this general picture.

OCRU ratio—Our simulation results in Figs. 2 and 4 show that increasing the OCRU ratio first promotes and then suppresses alternans. Increasing the OCRU ratio in a cell means that there are more CRUs lacking LCC clusters and thus less CRUs are available for primary sparks, which is equivalent to decreasing in α. In other words, a larger ϕ corresponds to a smaller a. Therefore, starting from a cell with no OCRUs (see the red arrow in Fig. 8A), since a is large, no alternans occurs. As the OCRU ratio increases, a decreases, which moves the cell into the alternans regime (gray zone in Fig. 8A), promoting alternans. As the OCRU ratio increases further, a may become too small, which moves the cell out of the alternans regime, suppressing alternans. This explains why alternans tends to occur in the intermediate range of the OCRU ratio ϕ.

Cell thickness—As shown in Fig. 2D, reducing the cell thickness causes a rightward shift (toward a higher ϕ) of the alternans regime. This is because a smaller cell exhibits a smaller total OCRU ratio given the same ϕ value (see Eq.1), resulting in an effectively larger a (Note that a smaller OCRU ratio corresponds to a larger a since more CRUs have their LCC clusters to fire as primary sparks). For example, for the case of ϕ=80%, a 64×32×16-CRU cell has a ϕ_{total}=64%, a 64×32×8-CRU cell has a ϕ_{total}=54%, and a 64x32x4-CRU cell has a ϕ_{total}=36%. Therefore, changing the cell thickness is equivalent to changing the total OCRU ratio, which affects alternans via changing a as indicated by the red arrow in Fig. 8A. Specifically, for a cell with a low ϕ (e.g., for 30%<ϕ<50% in Fig. 2D), a is in the range for alternans when the cell is thick, and reducing cell thickness moves the cell out of the alternans regime since a becomes too large. For a cell with a high ϕ (e.g., for ϕ>80% in Fig. 2D), a is too small for alternans when the cell is thick, and reducing cell thickness moves the cell into the alternans regime by increasing a.

TT structure heterogeneity—As shown in our simulations, it is more difficult for alternans to occur in the non- uniform TT networks for the same OCRU ratio ϕ (compare the cases for η=2 in Fig. 4 and Fig. 2). In the uniformly random TT networks, the LCC clusters are uniformly distributed, but are patchier in the non-uniform TT networks. An extreme case is a cell with only TT sheets, which effectively partition the cell into smaller cells, each with ϕ=100%. Therefore, changing the TT network from a homogeneous OCRU distribution to a heterogeneous OCRU distribution is equivalent to moving the cell into a higher ϕ regime. To directly show that the non-uniform TT networks are less susceptible to Ca^{2+} alternans than the uniformly random TT network, we carried out simulations in which the same number of LCC-NCX clusters were randomly distributed either only in the boundary CRUs or throughout the cell. Ca^{2+} alternans occurred in the cell with uniformly distributed LCC-NCX clusters but not in the non- uniform one (Fig. S8).

CRU coupling—CRU coupling strength depends on many factors, such as cytosolic and SR Ca^{2+} level, CRU distance, RyR sensitivity to Ca^{2+}, and Ca^{2+} diffusion. Increasing CRU coupling strength increases γ, which potentiates Ca^{2+} alternans (green arrow in Fig. 8A). In

both uniform and non-uniform TT networks, increasing CRU coupling strength by increasing η promotes alternans (see Figs. 2 and 4). This indicates that a shorter CRU distance (such as in failing VMs and in AMs) promotes alternans.

LCC cluster size and conductance—An interesting observation in Fig. 6 was that when ϕ=50%, increasing n_{LCC} always promoted alternans (see Fig. 6C), contrary to the case of no OCRUs in which increasing n_{LCC} eventually suppressed alternans (see Fig. 6A). Since the primary spark rate is determined by the coupling between the LCC cluster and the RyR cluster in a CRU, and thus α increases when the LCC conductance or the number (n_{LCC}) of LCCs in a CRU increases. In the case of no OCRUs (ϕ=0, the cyan arrow in Fig. 8A), when n_{LCC} is small, α is small and so no alternans occurs. Increasing n_{LCC} increases α, and also elevates the cytosolic Ca^{2+} level, which increases the probability (γ) of recruitment. The two effects are combined to promote alternans. However, increasing n_{LCC} further eventually causes all the CRUs to fire as primary sparks (α=1), which in turn moves the cell out of the alternans regime, suppressing alternans. In the case of ϕ=50% (the blue arrow in Fig. 8A), increasing n_{LCC} has the same effect on α and γ as for the case of ϕ=0. However, the difference is that increasing n_{LCC} can only increase α to around 0.5 since only 50% of the CRUs have their associated LCC clusters and can fire as primary sparks. Therefore, in this case, increasing n_{LCC} increases γ but can only increase α to ~0.5, which keeps the cell always in the alternans regime.

Mechanisms of subcellular spatially discordant alternans

Subcellular spatially discordant Ca^{2+} alternans have been observed in many experiments in both AMs [38, 42] and VMs [43–46]. One mechanism that has been proposed requires negative Ca^{2+}-to-voltage coupling [44, 47]. However, in our simulations the AP was clamped, which prohibited Ca^{2+}-to-voltage coupling. Therefore, the mechanism of negative Ca^{2+}-to-voltage coupling induced discordant alternans cannot apply to our case. As shown in our simulations, when there were no OCRUs, no spatially discordant alternans were observed although concordant Ca^{2+} alternans could occur in a certain range of $I_{Ca,L}$ (Fig. 6C). Spatially discordant alternans was potentiated by increasing the OCRU ratio (Figs. 3 and 6D) or by nonuniform TT networks (Fig. 4D). Not surprisingly, discordant alternans was suppressed by stronger CRU coupling (Figs. 3D and 4D) since stronger coupling promotes synchronous CRU firing. In experiments by Diaz et al. [43], spatially discordant Ca^{2+} alternans was observed under voltage clamp, and thus the mechanism of discordant alternans seen in this study may be applicable to the experimental observations.

TT network structures and mechanisms of triggered activity

The genesis of TA requires a large spontaneous Ca^{2+} transient and a large enough NCX current density to depolarize voltage to the threshold [48–50]. As shown in Fig. 7, a low NCX current density promotes spontaneous Ca^{2+} release but cannot depolarize the voltage to the threshold for TA. A high NCX current density supresses spontaneous Ca^{2+} release, and thus also prevents TA. However, in our simulations, although changing the OCRU ratio alters the whole-cell total L-type Ca^{2+} current and NCX current, it does not alter the current densities (see Eqs. S1 and S2, and Fig. S2) since the cell membrane capacitance was changed in proportional to the OCRU ratio. Therefore, changing the OCRU ratio or the TT

network structure has negligible direct effects on voltage depolarization. Moreover, altering the OCRUs ratio only has a minimal effect on SR Ca^{2+} load (see Fig. S6). Thus, the role of TT network structure in the genesis of TA is mainly via its effects on spontaneous Ca^{2+} release caused by the spatial distribution of the LCC-NCX clusters, as detailed below.

As shown in Fig. 8B, there is a competition between LCCs and NCX for the genesis of TA. A stronger NCX weakens CRU coupling, which suppresses the transition from sparks to spontaneous Ca^{2+} waves and synchronous Ca^{2+} release. A stronger $I_{Ca,L}$ promotes synchronous CRU firing in the paced AP and thus the recovery of the CRUs, which potentiates spontaneous Ca^{2+} release and a positive feedback between spontaneous Ca^{2+} release and voltage depolarization to promote TA as shown in our recent study [37]. *When the OCRU ratio is low* (e.g., Fig. 5A), the LCC-NCX clusters are densely and uniformly distributed throughout the cell. A densely distributed NCX effectively extrudes Ca^{2+}, making spontaneous Ca^{2+} release more difficult. Therefore, a low OCRU ratio makes TA less likely to occur. On the other hand, *when the OCRU ratio is high* (e.g., Fig. 5C), the LCC-NCX clusters are sparsely distributed in space, thus spontaneous Ca^{2+} release can occur more easily. However, a sparse LCC cluster distribution causes less synchronous CRU firing during the paced AP, resulting in less synchronous CRU recovery. Therefore, the amplitudes of the spontaneous Ca^{2+} transients are not high enough to elicit APs (Fig. 5C), which reduces the likelihood of TA. *When the OCRU ratio is in the intermediate range*, the LCC clusters and NCX are properly matched so that the CRUs can be sufficiently synchronized by the LCC clusters and spontaneous Ca^{2+} releases are not suppressed by NCX, potentiating TA.

For a thinner cell, the CRUs are more easily synchronized by the LCC clusters due to a smaller ϕ_{total}, and therefore more triggered APs can occur at high OCRU ratios as shown in Figs. 5 and 7. In non-uniform TT structures, OCRUs exhibit patchy distributions which causes less effective CRU synchronization than in uniformly random TT structures, and therefore fewer triggered APs were observed (Fig. 5F). A larger n_{LCC} enhances synchronous CRU firing to potentiate TA (Fig. 7).

Implications for arrhythmogenesis in different types of cardiac cells and remodeling in diseases

Different types of cardiac cells exhibit different characteristic TT network structures, RyR cluster spacing [28, 29], and cell sizes. Since the TT network structure and cell size play important roles in the genesis of Ca^{2+} alternans and TA, this may be responsible, at least partially, for different susceptibilities to arrhythmias of different types of cardiac cells and in remodeling. We illustrate this in Fig. 8C based on the modeling insights from this study and discuss the roles of TT network structure and cell thickness in the genesis of Ca^{2+} alternans and TA in detail below.

Normal ventricular myocytes—A normal VM exhibits a well-organized and dense TT network structure [1, 2]. As shown in our study, a well-organized and dense TT network structure is protective for both Ca^{2+} alternans and TA, and thus normal VMs are less susceptible to Ca^{2+} alternans and TA (Fig. 8C). However, Ca^{2+} alternans and TA can still

occur in normal VMs as have been widely shown in experiments since: 1) there are still OCRUs even in normal healthy VMs [2]; 2) Ca^{2+} alternans can be induced by blocking LCCs even in the absence of OCRUs [39]; and 3) Ca^{2+} waves and TA can occur due to Ca^{2+} overload [36].

Failing ventricular myocytes—Besides many other remodeling changes, the TTs in failing VMs are disrupted, which reduces the TT density and increases the heterogeneity of the TT network [2, 10–15]. As shown in this study (Figs.2D and 5D), reducing TT density alone can cause the failing VMs to be more susceptible to Ca^{2+} alternans and waves (Fig. 8C). Moreover, the RyR cluster distance becomes shorter in failing VMs [51], which also potentiates alternans and TA by enhancing C RU coupling as shown in our simulations (Figs.2,4, and 5). Note that as shown in many experimental studies, remodeled TT networks in failing VMs also become more heterogeneous, which may reduce the likelihood of alternans and TA based on our simulations. However, the shorter CRU spacing and lower TT density, as well as increased RyR leakiness, are all factors promoting alternans and TA, making failing VMs more susceptible to these arrhythmogenic dynamics.

Purkinje cells—P-cells are fairly large cells and lack TT networks. Based on our results, this makes it difficult to exhibit Ca^{2+} alternans (Fig. 8C). This may agree with the observation in a recent experimental study by Lee et al [52], in which no Ca^{2+} alternans but only irregular beat-to-beat Ca^{2+} transients were observed in the P-cells. On the other hand, lacking TTs may make Ca^{2+} waves occur more easily (see Figs.5 and 7), consistent with the observations that Ca^{2+} waves without TA have been shown in P-cells [53, 54].

Atrial myocytes—The TT networks in normal AMs are usually much more sparse than in normal VMs (Fig. 1D) [3], and are very heterogeneous across the atria in the same heart [17–20] and among species [21]. AMs are generally smaller than VMs and P-cells. As shown in an experimental study by Frisk et al [19], the TT networks are denser in larger AMs (as illustrated by the 3 representative AMs in Fig. 8C). Their less dense TT networks and size dependence make AMs more susceptible to Ca^{2+} alternans and TA than normal VMs, as illustrated in Fig. 8C. Note that although our results show that cells lacking TTs are less susceptible to alternans when the cell size is large, such as the P-cells, when the cell size is small, cells lacking TTs are still highly susceptible to alternans (left- lower quadrant of Fig. 8C), which is potentiated by enhanced CRU coupling (compare the two cases of η=3.33 and η=2 in Fig. 4 for ϕ=100%). Lacking TTs may also potentiate Ca^{2+} waves to result in Ca^{2+} alternans as shown in simulation by Li et al [55]. Therefore, AMs that exhibit sparse TT networks or lack TTs are highly susceptible to Ca^{2+} alternans, consistent with experimental findings that both concordant and discordant Ca^{2+} alternans have been widely observed in AMs [38, 42, 56–59]. However, the TT networks in AMs are also heterogeneous, which can also affect the susceptibility of AMs to alternans and TA.

Other cell types—Our current study has implications to other cell types as well. For example, in SAN cells, LCCs have been detected inside the cell volume [60], indicating that SAN cells may also exhibit a certain TT network structure. Our conclusion that an intermediate TT density promotes TA by enhancing the positive feedback between Ca^{2+}

release synchronization and AP excitation may also be applicable to SAN cells for potentiating oscillations and ensuring the robustness of pacemaking. Cultured or stem-cell derived cardiac myocytes lack TTs. Therefore, implications of Ca^{2+} alternans and Ca^{2+}-mediated TA observed in such experiments to arrhythmogenesis may need to be carefully interpreted.

Note that the placement of different type of cells in Fig. 8C is under the assumption that other conditions are the same. In the real heart, other differences among different types of cells exist, which may also play important roles in the genesis of Ca^{2+} alternans and TA. For example, I_{K1} is lower in AMs and P-cells than in VMs, and thus TA can occur at lower Ca^{2+} transient thresholds in AMs and P-cells than in VMs. The CRU spacing is shorter in AMs and failing VMs than in normal VMs, which also promotes Ca^{2+} alternans and TA. Fig. 8C only provides a schematic view of the roles of TT density and cell thickness in the susceptibility of different type of cardiac cells to Ca^{2+} alternans and TA. However, other differences still need to be considered when assessing the susceptibility of cardiac cells to these arrhythmogenic dynamics.

Limitations

We did not directly simulate the physical membrane structures of TT networks [61, 62] but represented them by a corresponding spatial distribution of the LCC-NCX clusters. We also did not consider other subcellular heterogeneities, such as RyR cluster size and heterogeneities [63]. We used uniform distributions of ion channels in both the sarcolemmal and TT membranes, which are non-uniform in the real cardiac cells. Since ion channel distribution are non- uniform, altering the TT network structure will also alter the whole-cell averaged current densities [64], and thus the action potentials, which can directly affect the AP dynamics, such as early afterdepolarizations in failing VMs [65]. Therefore, the effects of TT on susceptibility to arrhythmogenesis need to be considered under specific conditions. Another limitation is that it is not clear how to validate our theoretical predictions in vitro or in vivo experiments since techniques to provide systematic changes of TT density and structures are not readily available. Nevertheless, our study provides novel insights into the roles of TT network structure in the genesis of Ca^{2+} alternans and Ca^{2+}-mediated TA, which needs to be tested in future experiments.

Conclusions

Our simulations show that TT network structures play important roles in promoting Ca^{2+}-mediated arrhythmogenic dynamics, which may be responsible for the differential arrhythmia susceptibility in different types of cardiac cells and remodeling in cardiac diseases.

Supplementary Material

Refer to Web version on PubMed Central for supplementary material.

Acknowledgments

This work was supported by grants from National Institute of Health P01 HL078931, R01 HL133294, R56 HL110841, and F30 HL132449 (M.B.L).

References

1. Soeller C, Cannell MB. Examination of the Transverse Tubular System in Living Cardiac Rat Myocytes by 2-Photon Microscopy and Digital Image–Processing Techniques. Circ Res. 1999; 84:266–75. [PubMed: 10024300]
2. Song LS, Sobie EA, McCulle S, Lederer WJ, Balke CW, Cheng H. Orphaned ryanodine receptors in the failing heart. Proc Natl Acad Sci U S A. 2006; 103:4305–10. [PubMed: 16537526]
3. Brandenburg S, Kohl T, Williams GSB, Gusev K, Wagner E, Rog-Zielinska EA, et al. Axial tubule junctions control rapid calcium signaling in atria. The Journal of Clinical Investigation. 126:3999–4015.
4. Brette F, Orchard C. T-tubule function in mammalian cardiac myocytes. Circ Res. 2003; 92:1182–92. [PubMed: 12805236]
5. Dibb KM, Clarke JD, Eisner DA, Richards MA, Trafford AW. A functional role for transverse (t-) tubules in the atria. J Mol Cell Cardiol. 2013; 58:84–91. [PubMed: 23147188]
6. Hund TJ, Mohler PJ. Atrial-specific pathways for control of intracellular signaling and myocyte function. The Journal of Clinical Investigation. 2016; 126:3731–4. [PubMed: 27643440]
7. Legato MJ. Ultrastructure of the Atrial, Ventricular, and Purkinje Cell, with Special Reference to the Genesis of Arrhythmias. Circulation. 1973; 47:178–89. [PubMed: 4686595]
8. Ayettey AS, Navaratnam V. The T-tubule system in the specialized and general myocardium of the rat. J Anat. 1978; 127:125–40. [PubMed: 701190]
9. Chen B, Zhang C, Guo A, Song L-S. In situ single photon confocal imaging of cardiomyocyte T-tubule system from Langendorff-perfused hearts. Frontiers in Physiology. 2015:6.
10. Lyon AR, MacLeod KT, Zhang Y, Garcia E, Kanda GK, Lab MJ, et al. Loss of T-tubules and other changes to surface topography in ventricular myocytes from failing human and rat heart. Proc Natl Acad Sci U S A. 2009; 106:6854–9. [PubMed: 19342485]
11. Wei S, Guo A, Chen B, Kutschke W, Xie YP, Zimmerman K, et al. T-tubule remodeling during transition from hypertrophy to heart failure. Circ Res. 2010; 107:520–31. [PubMed: 20576937]
12. Sachse FB, Torres NS, Savio-Galimberti E, Aiba T, Kass DA, Tomaselli GF, et al. Subcellular structures and function of myocytes impaired during heart failure are restored by cardiac resynchronization therapy. Circ Res. 2012; 110:588–97. [PubMed: 22253411]
13. Li H, Lichter JG, Seidel T, Tomaselli GF, Bridge JHB, Sachse FB. Cardiac Resynchronization Therapy Reduces Subcellular Heterogeneity of Ryanodine Receptors, T-Tubules, and Ca^{2+} Sparks Produced by Dyssynchronous Heart Failure. Circulation: Heart Failure. 2015; 8:1105–14. [PubMed: 26294422]
14. Guo A, Zhang C, Wei S, Chen B, Song L-S. Emerging mechanisms of T-tubule remodelling in heart failure. Cardiovasc Res. 2013; 98:204–15. [PubMed: 23393229]
15. Seidel T, Navankasattusas S, Ahmad AA, Diakos NA, Xu WD, Tristani-Firouzi M, et al. Sheet-Like Remodeling of the Transverse Tubular System in Human Heart Failure Impairs Excitation-Contraction Coupling and Functional Recovery by Mechanical Unloading. Circulation. 2017
16. Dibb KM, Clarke JD, Horn MA, Richards MA, Graham HK, Eisner DA, et al. Characterization of an Extensive Transverse Tubular Network in Sheep Atrial Myocytes and its Depletion in Heart Failure. Circulation: Heart Failure. 2009; 2:482–9. [PubMed: 19808379]
17. Kirk MM, Izu LT, Chen-Izu Y, McCulle SL, Wier WG, Balke CW, et al. Role of the transverse-axial tubule system in generating calcium sparks and calcium transients in rat atrial myocytes. J Physiol. 2003; 547:441–51. [PubMed: 12562899]
18. Arora R, Aistrup GL, Supple S, Frank C, Singh J, Tai S, et al. Regional distribution of T-tubule density in left and right atria in dogs. Heart Rhythm. 2016 (in press).

19. Frisk M, Koivumäki JT, Norseng PA, Maleckar MM, Sejersted OM, Louch WE. Variable t-tubule organization and Ca^{2+} homeostasis across the atria. American Journal of Physiology - Heart and Circulatory Physiology. 2014; 307:H609–H20. [PubMed: 24951751]
20. Glukhov AV, Balycheva M, Sanchez-Alonso JL, Ilkan Z, Alvarez-Laviada A, Bhogal N, et al. Direct Evidence for Microdomain-Specific Localization and Remodeling of Functional L-Type Calcium Channels in Rat and Human Atrial Myocytes. Circulation. 2015; 132:2372–84. [PubMed: 26450916]
21. Richards MA, Clarke JD, Saravanan P, Voigt N, Dobrev D, Eisner DA, et al. Transverse tubules are a common feature in large mammalian atrial myocytes including human. Am J Physiol Heart Circ Physiol. 2011; 301:H1996–2005. [PubMed: 21841013]
22. Boyden PA, Albala A, Dresdner KP. Electrophysiology and ultrastructure of canine subendocardial Purkinje cells isolated from control and 24-hour infarcted hearts. Circ Res. 1989; 65:955–70. [PubMed: 2791230]
23. Di Maio A, Ter Keurs HE, Franzini-Armstrong C. T-tubule profiles in Purkinje fibres of mammalian myocardium. J Muscle Res Cell Motil. 2007; 28:115–21. [PubMed: 17572852]
24. Chen F, Mottino G, Klitzner TS, Philipson KD, Frank JS. Distribution of the Na+/Ca2+ exchange protein in developing rabbit myocytes. American Journal of Physiology - Cell Physiology. 1995; 268:C1126–C32.
25. Lipp P, Hüser J, Pott L, Niggli E. Spatially non-uniform Ca2+ signals induced by the reduction of transverse tubules in citrate- loaded guinea-pig ventricular myocytes in culture. The Journal of Physiology. 1996; 497:589–97. [PubMed: 9003546]
26. Lieu DK, Liu J, Siu C-W, McNerney GP, Tse H-F, Abu-Khalil A, et al. Absence of Transverse Tubules Contributes to Non-Uniform Ca2+ Wavefronts in Mouse and Human Embryonic Stem Cell–Derived Cardiomyocytes. Stem Cells and Development. 2009; 18:1493–500. [PubMed: 19290776]
27. Liu J, Lieu DK, Siu CW, Fu J-D, Tse H-F, Li RA. Facilitated maturation of Ca^{2+} handling properties of human embryonic stem cell-derived cardiomyocytes by calsequestrin expression. American Journal of Physiology - Cell Physiology. 2009; 297:C152–C9. [PubMed: 19357236]
28. Chen-Izu Y, McCulle SL, Ward CW, Soeller C, Allen BM, Rabang C, et al. Three-dimensional distribution of ryanodine receptor clusters in cardiac myocytes. Biophys J. 2006; 91:1–13. [PubMed: 16603500]
29. Stern MD, Maltseva LA, Juhaszova M, Sollott SJ, Lakatta EG, Maltsev VA. Hierarchical clustering of ryanodine receptors enables emergence of a calcium clock in sinoatrial node cells. The Journal of General Physiology. 2014; 143:577–604. [PubMed: 24778430]
30. Izu LT, Means SA, Shadid JN, Chen-Izu Y, Balke CW. Interplay of ryanodine receptor distribution and calcium dynamics. Biophys J. 2006; 91:95–112. [PubMed: 16603499]
31. Nivala M, Ko CY, Nivala M, Weiss JN, Qu Z. Criticality in intracellular calcium signaling in cardiac myocytes. Biophys J. 2012; 102:2433–42. [PubMed: 22713558]
32. Nivala M, Ko CY, Nivala M, Weiss JN, Qu Z. The Emergence of Subcellular Pacemaker Sites for Calcium Waves and Oscillations. J Physiol. 2013; 591:5305–20. [PubMed: 24042497]
33. Nivala M, Song Z, Weiss JN, Qu Z. T-tubule disruption promotes calcium alternans in failing ventricular myocytes: Mechanistic insights from computational modeling. J Mol Cell Cardiol. 2015; 79:32–41. [PubMed: 25450613]
34. Orchard CH, Bryant SM, James AF. Do t-tubules play a role in arrhythmogenesis in cardiac ventricular myocytes? The Journal of Physiology. 2013; 591:4141–7. [PubMed: 23652596]
35. Song Z, Karma A, Weiss JN, Qu Z. Long-Lasting Sparks: Multi-Metastability and Release Competition in the Calcium Release Unit Network. PLoS Comput Biol. 2016; 12:e1004671. [PubMed: 26730593]
36. Song Z, Ko CY, Nivala M, Weiss James N, Qu Z. Calcium- Voltage Coupling in the Genesis of Early and Delayed Afterdepolarizations in Cardiac Myocytes. Biophys J. 2015; 108:1908–21. [PubMed: 25902431]
37. Song Z, Qu Z, Karma A. Stochastic initiation and termination of calcium- mediated triggered activity in cardiac myocytes. Proceedings of the National Academy of Sciences. 2017; 114:E270–E9.

38. Blatter LA, Kockskamper J, Sheehan KA, Zima AV, Huser J, Lipsius SL. Local calcium gradients during excitation-contraction coupling and alternans in atrial myocytes. J Physiol. 2003; 546:19–31. [PubMed: 12509476]
39. Rovetti R, Cui X, Garfinkel A, Weiss JN, Qu Z. Spark-Induced Sparks As a Mechanism of Intracellular Calcium Alternans in Cardiac Myocytes. Circ Res. 2010; 106:1582–91. [PubMed: 20378857]
40. Nivala M, Qu Z. Calcium Alternans in a Couplon Network Model of Ventricular Myocytes: Role of Sarcoplasmic Reticulum Load. Am J Physiol Heart Circ Physiol. 2012; 303:H341–52. [PubMed: 22661509]
41. Qu Z, Liu MB, Nivala M. A unified theory of calcium alternans in ventricular myocytes. Scientific reports. 2016; 6:35625. [PubMed: 27762397]
42. Song Z, Adam K, Backx PH, Qu Z. Subcellular Ca Channel Distribution and Ca Alternans in Atrial Myocytes. Biophys J. 2015; 108:261a. [PubMed: 25606675]
43. Diaz ME, Eisner DA, O'Neill SC. Depressed ryanodine receptor activity increases variability and duration of the systolic Ca2+ transient in rat ventricular myocytes. Circ Res. 2002; 91:585–93. [PubMed: 12364386]
44. Gaeta SA, Bub G, Abbott GW, Christini DJ. Dynamical mechanism for subcellular alternans in cardiac myocytes. Circ Res. 2009; 105:335–42. [PubMed: 19628792]
45. Xie LH, Weiss JN. Arrhythmogenic consequences of intracellular calcium waves. Am J Physiol Heart Circ Physiol. 2009; 297:H997–H1002. [PubMed: 19561309]
46. Aistrup GL, Shiferaw Y, Kapur S, Kadish AH, Wasserstrom JA. Mechanisms underlying the formation and dynamics of subcellular calcium alternans in the intact rat heart. Circ Res. 2009; 104:639–49. [PubMed: 19150887]
47. Shiferaw Y, Karma A. Turing instability mediated by voltage and calcium diffusion in paced cardiac cells. Proc Natl Acad Sci U S A. 2006; 103:5670–5. [PubMed: 16574775]
48. Schlotthauer K, Bers DM. Sarcoplasmic reticulum Ca(2+) release causes myocyte depolarization. Underlying mechanism and threshold for triggered action potentials. Circ Res. 2000; 87:774–80. [PubMed: 11055981]
49. Maruyama M, Joung B, Tang L, Shinohara T, On YK, Han S, et al. Diastolic intracellular calcium-membrane voltage coupling gain and postshock arrhythmias: role of purkinje fibers and triggered activity. Circ Res. 2010; 106:399–408. [PubMed: 19926871]
50. Liu BM, Ko CY, Song Z, Garfinkel A, Weiss JN, Qu Z. A Dynamical Threshold for the Cardiac Action Potential: Implications for Delayed Afterdepolarization-Mediated Triggered Activity. Biophys J. 2016 (in press).
51. Chen-Izu Y, Ward CW, Stark W Jr, Banyasz T, Sumandea MP, Balke CW, et al. Phosphorylation of RyR2 and shortening of RyR2 cluster spacing in spontaneously hypertensive rat with heart failure. Am J Physiol Heart Circ Physiol. 2007; 293:H2409–17. [PubMed: 17630346]
52. Lee YS, Dun W, Boyden PA, Sobie EA. Complex and rate-dependent beat-to-beat variations in Ca(2+) transients of canine Purkinje cells. J Mol Cell Cardiol. 2011:662–9. [PubMed: 21232541]
53. Boyden PA, Pu J, Pinto J, Keurs HE. Ca(2+) transients and Ca(2+) waves in purkinje cells: role in action potential initiation. Circ Res. 2000; 86:448–55. [PubMed: 10700450]
54. Boyden PA, Hirose M, Dun W. Cardiac Purkinje cells. Heart Rhythm. 2010; 7:127–35. [PubMed: 19939742]
55. Li Q, O'Neill SC, Tao T, Li Y, Eisner D, Zhang H. Mechanisms by which cytoplasmic calcium wave propagation and alternans are generated in cardiac atrial myocytes lacking T-tubules-insights from a simulation study. Biophys J. 2012; 102:1471–82. [PubMed: 22500747]
56. Huser J, Wang YG, Sheehan KA, Cifuentes F, Lipsius SL, Blatter LA. Functional coupling between glycolysis and excitation-contraction coupling underlies alternans in cat heart cells. J Physiol. 2000; 524(Pt 3):795–806. [PubMed: 10790159]
57. Kockskamper J, Blatter LA. Subcellular Ca2+ alternans represents a novel mechanism for the generation of arrhythmogenic Ca2+ waves in cat atrial myocytes. J Physiol. 2002; 545:65–79. [PubMed: 12433950]

58. Shkryl VM, Maxwell JT, Domeier TL, Blatter LA. Refractoriness of sarcoplasmic reticulum Ca release determines Ca alternans in atrial myocytes. American Journal of Physiology - Heart and Circulatory Physiology. 2012; 302:H2310–H20. [PubMed: 22467301]
59. Llach A, Molina CE, Fernandes J, Padró J, Cinca J, Hove-Madsen L. Sarcoplasmic reticulum and L-type Ca2+ channel activity regulate the beat-to-beat stability of calcium handling in human atrial myocytes. The Journal of Physiology. 2011; 589:3247–62. [PubMed: 21521767]
60. Christel CJ, Cardona N, Mesirca P, Herrmann S, Hofmann F, Striessnig J, et al. Distinct localization and modulation of Cav1.2 and Cav1.3 L-type Ca2+ channels in mouse sinoatrial node. The Journal of Physiology. 2012; 590:6327–41. [PubMed: 23045342]
61. Colman MA, Pinali C, Trafford AW, Zhang H, Kitmitto A. A computational model of spatio-temporal cardiac intracellular calcium handling with realistic structure and spatial flux distribution from sarcoplasmic reticulum and t-tubule reconstructions. PLOS Computational Biology. 2017; 13:e1005714. [PubMed: 28859079]
62. Cheng Y, Yu Z, Hoshijima M, Holst MJ, McCulloch AD, McCammon JA, et al. Numerical Analysis of Ca2+ Signaling in Rat Ventricular Myocytes with Realistic Transverse-Axial Tubular Geometry and Inhibited Sarcoplasmic Reticulum. PLOS Computational Biology. 2010; 6:e1000972. [PubMed: 21060856]
63. Rajagopal V, Bass G, Walker CG, Crossman DJ, Petzer A, Hickey A, et al. Examination of the Effects of Heterogeneous Organization of RyR Clusters, Myofibrils and Mitochondria on Ca2+ Release Patterns in Cardiomyocytes. PLOS Computational Biology. 2015; 11:e1004417. [PubMed: 26335304]
64. Bryant SM, Kong CHT, Watson J, Cannell MB, James AF, Orchard CH. Altered distribution of I_{Ca} impairs Ca release at the t-tubules of ventricular myocytes from failing hearts. J Mol Cell Cardiol. 86:23–31.
65. Sanchez-Alonso JL, Bhargava A, O'Hara T, Glukhov AV, Schobesberger S, Bhogal N, et al. Microdomain-Specific Modulation of L-Type Calcium Channels Leads to Triggered Ventricular Arrhythmia in Heart Failure. Circ Res. 2016; 119:944–55. [PubMed: 27572487]
66. Cordeiro JM, Spitzer KW, Giles WR, Ershler PE, Cannell MB, Bridge JH. Location of the initiation site of calcium transients and sparks in rabbit heart Purkinje cells. J Physiol. 2001; 531:301–14. [PubMed: 11310434]

Highlights

- T-tubular density and structure are heterogeneous among different types of cardiac cells.
- T-tubular networks in failing ventricular myocytes are disrupted and become more heterogeneous.
- Ca^{2+} alternans and triggered activity are promoted by intermediate T-tubular density.
- Susceptibility to alternans and triggered activity depends on the T-tubular network heterogeneity.
- The T-tubular difference in different cell types may contribute to their difference in susceptibility to alternans and triggered activity.

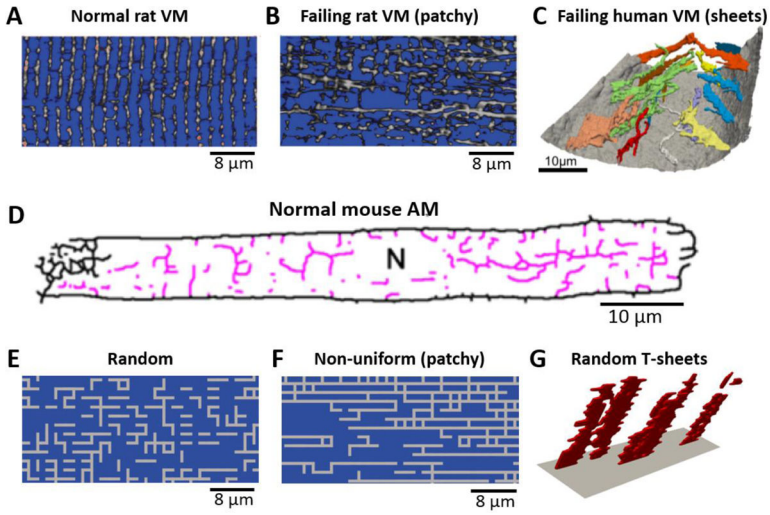

Figure 1. TT network structures observed in VMs and AMs and computer generated TT network structures

A. TT network structure in a normal rat VM (Song et al. [2]). **B**. TT network in a failing rat VM (Song et al. [2]). **C**. Sheet-like TT structure in a failing human VM (Seidel et al. [15]). **D**. TT network in a normal mouse AM (Brandenburg et al. [3]). **E**. A computer generated uniformly random TT network. **F**. A computer generated non-uniformly random TT network (AT-to-TT ratio=~3). **G**. A computer generated sheet-like TT structure.

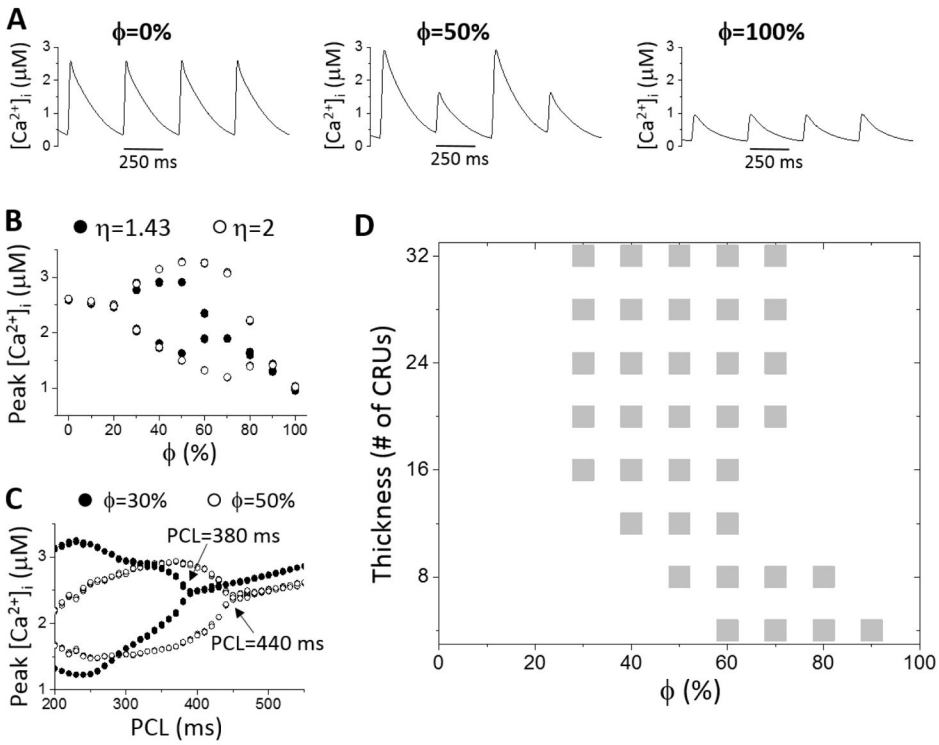

Figure 2. Effect of OCRU ratio and cell size on Ca^{2+} alternans

A. $[Ca^{2+}]_i$ versus time for ϕ=0, 50%, and 100%. PCL=360 ms. L_z=16 CRUs. **B**. Peak $[Ca^{2+}]_i$ versus ϕ for η=2 (open circle) and 1.43 (filled circle). PCL=360 ms. L_z=16 CRUs. **C**. Peak $[Ca^{2+}]_i$ versus PCL for ϕ=30% (filled circle) and 50% (open circle). L_z=16 CRUs. Arrows indicate the onset of Ca^{2+} alternans. **D**. Occurrence of Ca^{2+} alternans (gray boxes) versus cell thickness and ϕ.

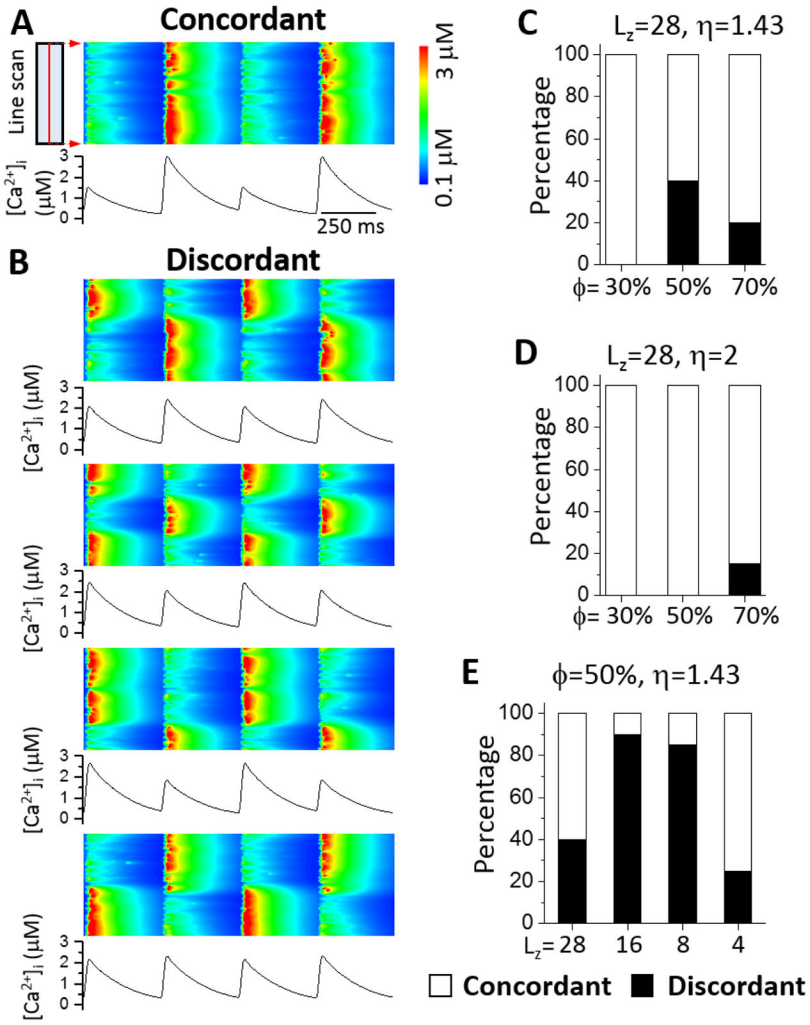

Figure 3. Spatially discordant Ca^{2+} alternans

A. Line scan and $[Ca^{2+}]_i$ from a simulation showing spatially concordant alternans. **B**. Line scans and $[Ca^{2+}]_i$ from simulations of 4 different TT network structures showing spatially discordant alternans. **C**. Percentage of discordant alternans for three ϕ values with L_z=28 CRUs and η=1.43. **D**. Percentage of discordant alternans for three ϕ values with L_z=28 CRUs and η=2. **E**. Percentage of discordant alternans for different cell thickness with ϕ=50% and η=1.43. For each bar in C–E, 20 simulations were performed with different randomly generated TT network structures.

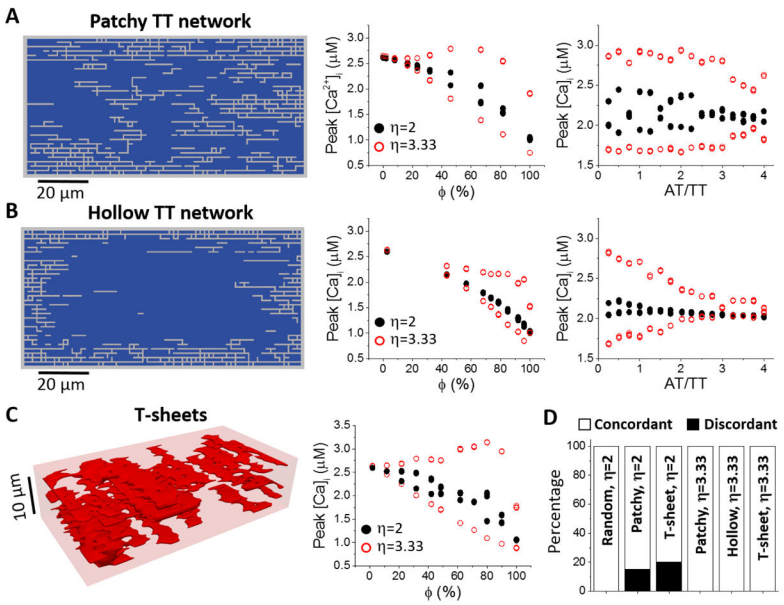

Figure 4. Effects of different non-uniform TT network structures on Ca^{2+} alternans

A. *Patchy TT networks* (random walk length was 360 steps). Left: A 2D slice from a generated 3D TT network. The slice is normal to the Z- line and is the 7th layer in a total of 16 layers along the Z- line. Middle: Peak $[Ca]_i$ versus ϕ for AT/TT=3. Right: Peak $[Ca^{2+}]_i$ versus AT/TT ratio for ϕ~50%. PCL=360 ms. Since ϕ is not a preset parameter, we generated random TT networks with ϕ between 48% and 52%. **B**. *Hollow TT networks* (random walk length was 72 steps). Plots are the same as in A. **C**. *T-sheet structures*. Left: An example of sheet- like TT structure. Right: peak $[Ca^{2+}]_i$ versus ϕ for η=2 and 3.33. **D**. Percentage of discordant alternans for different types of TT network structures and η values as indicated. In all cases, ϕ=50%±2%. For each case, we performed 20 simulations with different randomly generated TT network structures.

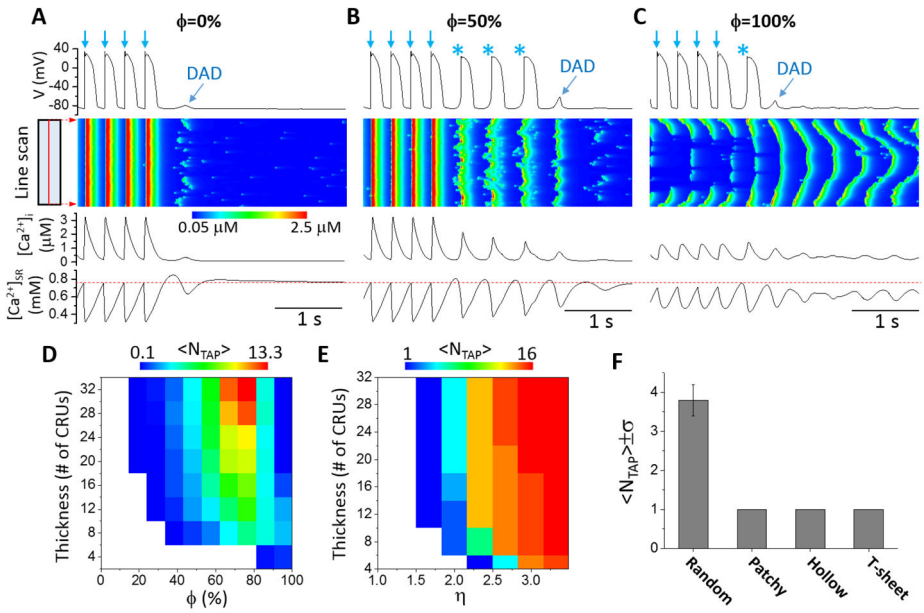

Figure 5. Effects of OCRU ratio on Ca^{2+} waves and TA

Time traces of membrane potential, $[Ca^{2+}]_i$, and $[Ca^{2+}]_{SR}$, with line-scan images of cytosolic Ca^{2+} concentration for uniformly random TT network structures with **A**. ϕ=0, **B**. ϕ= 50%, and **C**. ϕ=100%. The line-scans are taken from the center axis along the longitudinal direction. **D**. Dependence of $<N_{T\ AP}>$ on cell thickness and ϕ. **E**. Dependence of $<N_{T\ AP}>$ on cell thickness and η. ϕ=50%. The simulation protocol was the same as in D. **F**. $<N_{T\ AP}>$ for different types of TT network structures: uniform, patchy, hollow, and T-sheet. The value of $<N_{T\ AP}>$ in the above panels was obtained from 10 independent simulations, each with a randomly generated TT network structure.

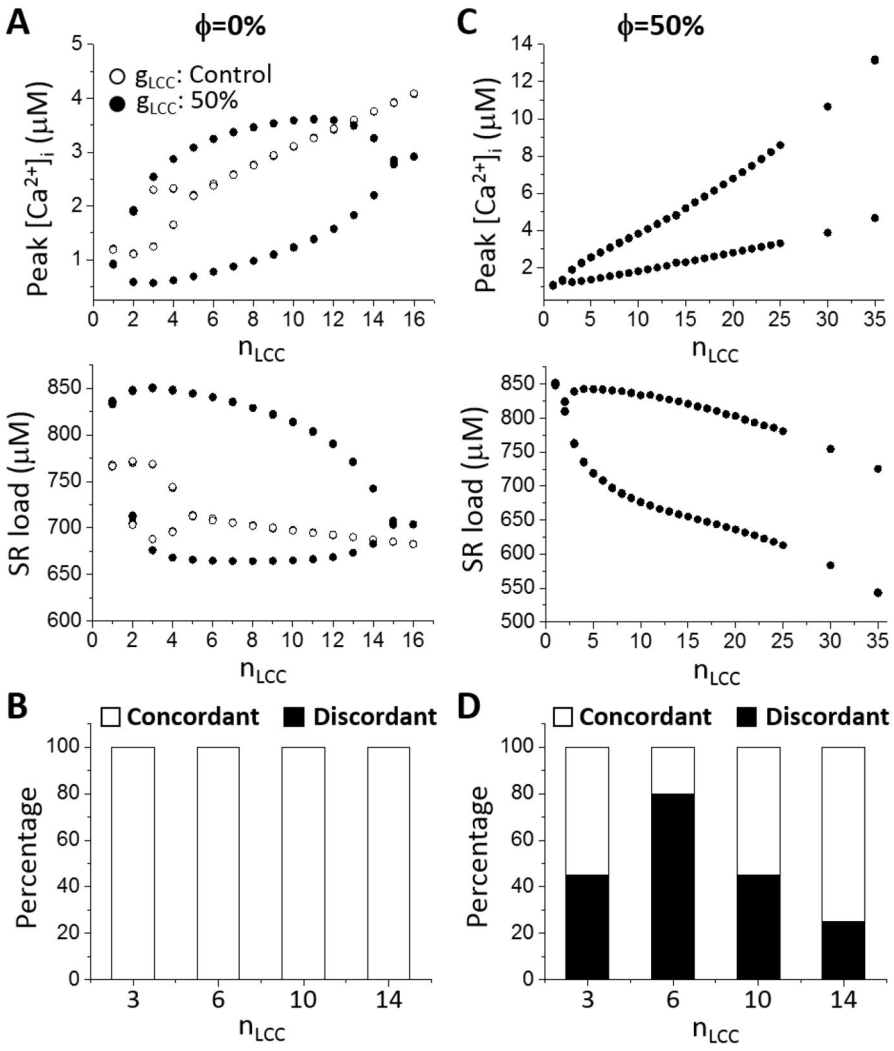

Figure 6. Effects of LCC cluster size on Ca^{2+} alternans

A. Bifurcation diagrams of peak $[Ca^{2+}]_i$ (top) and SR Ca^{2+} load (bottom) versus LCC cluster size (n_{LCC}) for control g_{LCC} (open circle) and 50% g_{LCC} block (filled circle) with ϕ=0. **B**. Bifurcation diagrams of peak $[Ca^{2+}]_i$ (top) and SR Ca^{2+} load (bottom) versus LCC cluster size with control g_{LCC} and ϕ=50%. **C**. Percentage of concordant and discordant alternans for n_{LCC}=3, 6, 10, and 14 with ϕ=0. **D**. Same as in C, but with ϕ=50%. Cell thickness was L_z=32 CRUs. PCL=300 ms. For each n_{LCC}, 20 simulations were performed, each with a randomly generated uniform TT network structure.

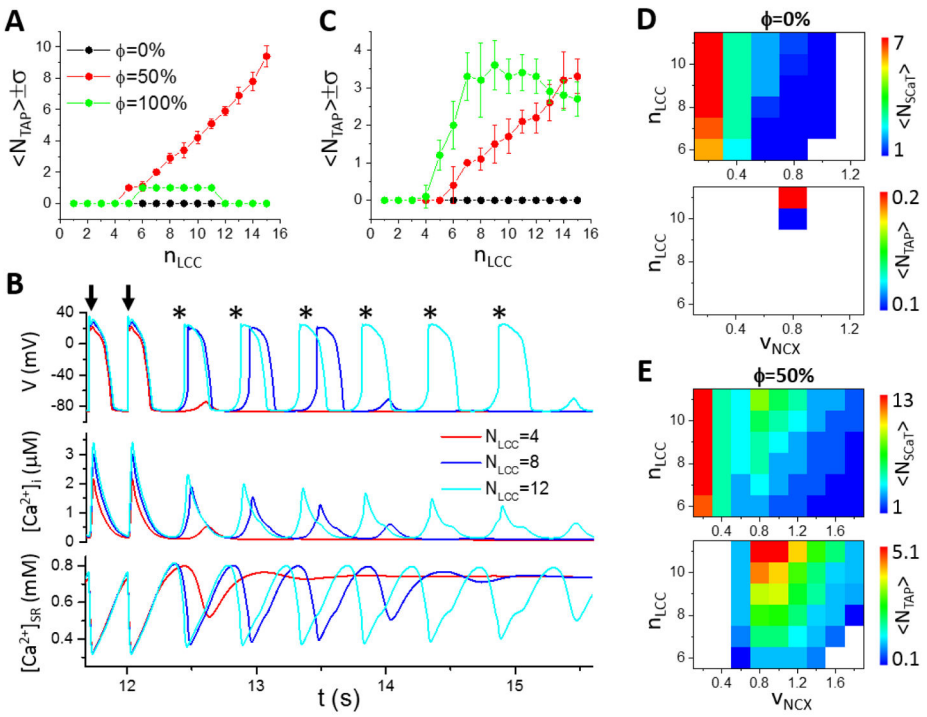

Figure 7. Effects of LCC cluster size and NCX strength on TA

A. $<N_{T\ AP}>$ versus n_{LCC} for ϕ=0 (black), 50% (red) and 100% (green). L_z=32 CRUs. Error bars indicate the standard deviation over 10 simulations. **B**. Time traces of membrane potential (top), $[Ca^{2+}]_i$, (middle), and $[Ca^{2+}]_{SR}$ (bottom) for n_{LCC}=4, 8 and 12 with ϕ=50% as in A. Arrows indicate paced beats. Triggered APs are marked by *. **C**. Same as in A, but L_z= 8 CRUs. **D**. Spontaneous Ca^{2+} release and TA for ϕ=0. For each parameter set (n_{LCC} and v_{NCX}), $<N_{SCaT}>$ and $<N_{T\ AP}>$ were obtained by performing 20 simulations, each with a randomly generated uniform TT network structure. Upper: $<N_{SCaT}>$ versus n_{LCC} and v_{NCX}. Lower: $<N_{T\ AP}>$ versus n_{LCC} and v_{NCX}. **E**. Same as D but for ϕ=50%.

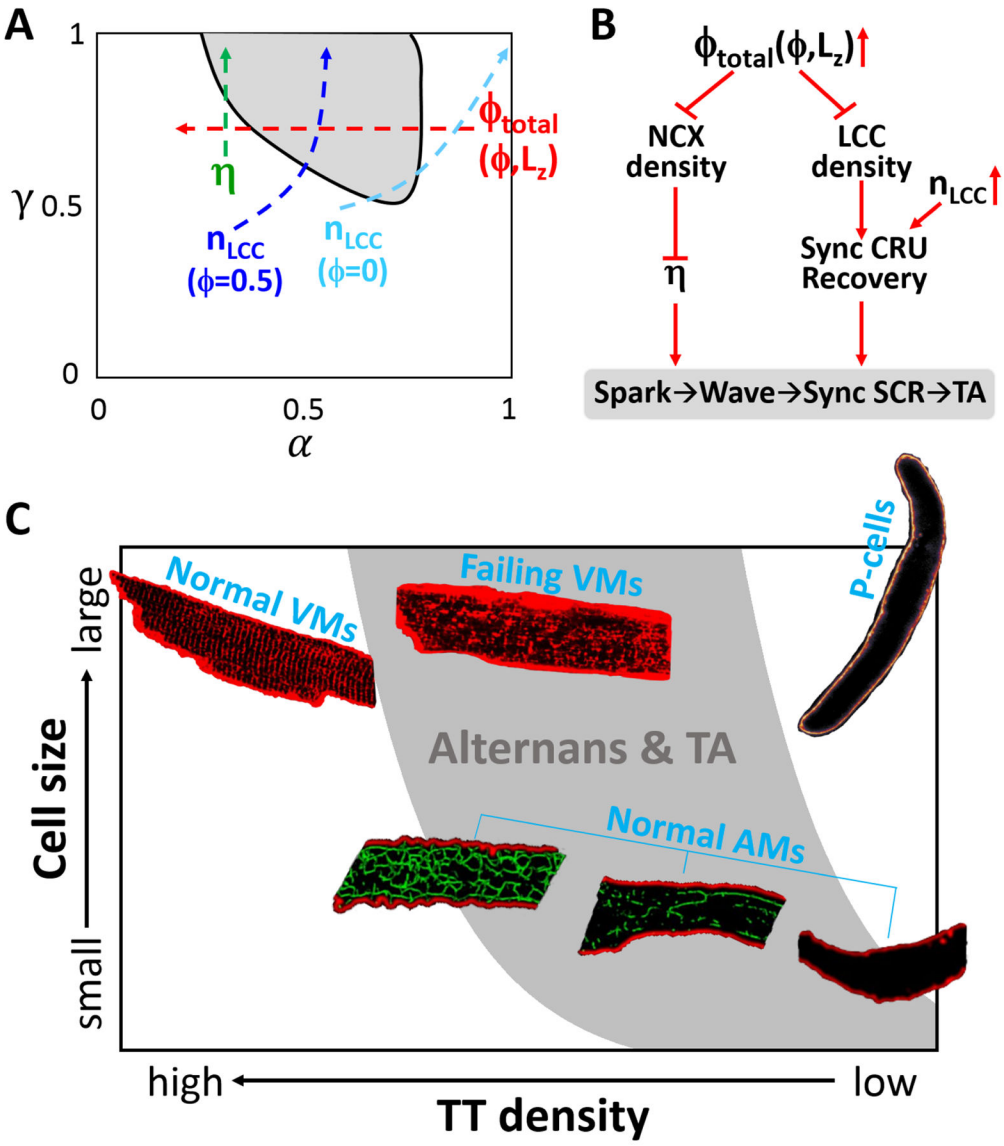

Figure 8. Schematic diagrams. A. TT network structure and mechanism of Ca^{2+} alternans The gray region is the region of alternans in the α-γ parameter space predicted by the theory. Red arrow indicates increasing ϕ_{total} which depends on ϕ and L_z. For a cell with ϕ>0, decreasing L_z decreases ϕ_{total} according to Eqs. 1 and 2. Green arrows indicates increasing CRU coupling. Blue arrow indicates increasing n_{LCC} when ϕ=50%. Cyan arrow indicates increasing n_{LCC} when ϕ=0. **B. TT network structure and mechanism of Ca^{2+}-wave mediated TA**. Increasing the OCRU ratio (ϕ_{total}) reduces both NCX density and LCC density. Reducing spatial density of NCX enhances CRU coupling, potentiating the spark-to-wave transition and synchronized whole-cell spontaneous Ca^{2+} release and thus TA. Reducing the spatial density of the LCC clusters weakens CRU synchronization and the positive feedback between spontaneous Ca^{2+} release, suppressing TA. Therefore, changing the OCRU ratio promotes a competition process which causes TA to occur in the intermediate range of OCRU ratio. **C. Susceptibilities of different type of cardiac cells to**

Ca^{2+} alternans and TA based on their TT network and size characteristics. The gray zone indicates the high incidence regime of Ca^{2+} alternans and TA based on simulation results shown in Fig. 2D and Fig. 5D. Each cell type is placed in a representative location based on their typically observed TT-network densities and cell sizes. The images of normal and failing VMs with TT structures were modified from Chen et al [9]; the images of P-cell was from Cordeiro et al [66]; and the images of AMs with TT structures were from Frisk et al [19]. Based on the experimental observations of Frisk et al, the TT networks are denser in larger AMs as represented by the 3 AM images.